Full Paper submitted to: Magnetic Resonance in Medicine → Computer Processing and Modeling

Global Sensitivity Analysis of Skeletal Muscle dMRI Metrics: Effects of Microstructural and Pulse Parameters

Noel M. Naughton[1] and **John G. Georgiadis**[1,2]

[1]Department of Mechanical Science and Engineering, University of Illinois at Urbana-Champaign, Urbana IL, USA;

[2]Department of Biomedical Engineering, Illinois Institute of Technology, Chicago IL, USA

Contact Information:

Noel M. Naughton
Mechanical Engineering Building,
1206 W Green St,
Urbana, IL 61801, USA
nnaught2@illinois.edu

John G. Georgiadis (Corresponding Author)
3255 South Dearborn Street
Wishnick Hall, Suite 314
Chicago, IL 60616, USA
jgeorgia@iit.edu

Abstract

Purpose: Estimating microstructural parameters of skeletal muscle from diffusion MRI (dMRI) signal requires understanding the relative importance of both microstructural and dMRI sequence parameters on the signal. This study seeks to determine the sensitivity of dMRI signal to variations in microstructural and dMRI sequence parameters, as well as assess the effect of noise on sensitivity.

Methods: Using a cylindrical myocyte model of skeletal muscle, numerical solutions of the Bloch-Torrey equation were used to calculate global sensitivity indices of dMRI metrics (FA, RD, MD, λ_1, λ_2, λ_3) for wide ranges of microstructural and dMRI sequence parameters. The microstructural parameters were: myocyte diameter, volume fraction, membrane permeability, intra- and extracellular diffusion coefficients, and intra- and extracellular T_2 times. Two separate pulse sequences were examined, a PGSE and a generalized diffusion-weighted sequence that accommodates a larger range of diffusion times. The effect of noise and signal averaging on the sensitivity of the dMRI metrics was examined by adding synthetic noise to the simulated signal.

Results: Among the examined parameters, the intracellular diffusion coefficient has the strongest effect, and myocyte diameter is more influential than permeability for FA and RD. The sensitivity indices do not vary significantly between the two pulse sequences. Also, noise strongly affects the sensitivity of the dMRI signal to microstructural variations.

Conclusion: With the identification of key microstructural features that affect dMRI measurements, the reported sensitivity results can help interpret dMRI measurements of skeletal muscle in terms of the underlying microstructure and further develop parsimonious dMRI models of skeletal muscle.

Keywords: sensitivity analysis; Bloch-Torrey equation; lattice Boltzmann method; diffusion MRI; skeletal muscle

Word count: 5393/5000

Figures: 4/10

1 Introduction

Changes in skeletal muscle pathology are associated with changes in the tissue microstructure. Examples include increased fibrosis due to injury and muscular dystrophy [1], changes in fiber type and cross-sectional area due to aging [2, 3], and increased membrane permeability due to sarcolemma damage from muscular dystrophy [4, 5]. Measuring these microstructural changes is necessary to better understand these pathologies, however, such measurements are difficult to obtain. Muscle excision and sectioning for histological analysis is invasive and time consuming. Excision and sectioning may also change the morphological features being examined [6]. Diffusion MRI (dMRI) is a promising noninvasive method that is sensitive to changes in the underlying microstructure. Much work has been done in brain matter to elucidate the relationship between the dMRI signal and the underlying microstructure [7]. dMRI can be similarly applied to skeletal muscle, however, this relationship is less understood due in large part to difficulties in signal acquisition caused by the relatively short T_2 of skeletal muscle [8]. Additionally, the larger cell size and dense packing of muscle fibers makes some popular white matter tissue models inappropriate for use in skeletal muscle [9].

Skeletal muscle consists of an ordered, hierarchical organization of muscle cells surrounded by an extracellular collagen matrix (endomysium) and bundled together into fascicles, which are themselves bundled to form the whole muscle. This organization has short range order and can be abstracted as a periodic cylinder array characterized by a representative elementary volume (REV). This REV can be easily parameterized to allow systematic investigation of how changes in the REV effect the dMRI signal. Others have examined structural variations in such geometries using Monte Carlo simulations [10–12], however, a comprehensive analysis of how microstructural and pulse parameters affect the dMRI signal has not been reported. Further, there are conflicting reports regarding the relative influence of membrane permeability and fiber diameter [10, 11]. Previous studies have examined either a limited number of microstructural and pulse parameters or used a limited number of parameter combinations. As such, it is uncertain whether the reported sensitivity relationships represent the global influence of a parameter or if they reflect local interactions dependent on other parameters. To address this uncertainty, we identify seven microstructural parameters that we believe comprehensively parameterize muscle microstructure, as well as two dMRI sequence parameters, and examine the sensitivity of dMRI signal to these parameters. Using a lattice Boltzmann method solution of the Bloch-Torrey equation applied to the above-mentioned muscle REV, we perform a global sensitivity analysis of the influence that microstructural and dMRI sequence parameters have on dMRI metrics, such as fractional anisotropy (FA), mean diffusivity (MD), and radial diffusivity (RD). This analysis comprehensively

samples all possible combinations of these parameters to determine which ones have the largest effect on dMRI metrics. The results will assist in the proper parameterization of dMRI muscle tissue models so that microstructural parameters can be extracted by interpreting the dMRI signal.

The aim of the present work is to determine the sensitivity of dMRI signal to variations in microstructural and dMRI sequence parameters. Additionally, we assess the effect of noise on the sensitivity relationships in order to determine a minimum SNR level that will allow the correct interpretation of skeletal muscle dMRI signal. While similar aims have been addressed previously [10–12], a wider range of both microstructural and pulse parameters is examined here in order to identify key sensitivity relationships. This includes analysis of the sensitivity of the dMRI signal to compartment-specific diffusion coefficients as well as a broad range of sarcolemma permeability values, both not addressed before. The present sensitivity analysis will help interpret dMRI measurements in terms of the underlying microstructural tissue parameters, and will also inform further model development by identifying low sensitivity microstructural parameters, thus allowing a reduction in the number of requisite independent model parameters.

2 Methods

dMRI Signal Representation

The fate of dMRI signal is described by the Bloch-Torrey equation [13]

$$\frac{\partial \boldsymbol{M}(\boldsymbol{x},t)}{\partial t} = -i(\gamma \boldsymbol{G}(t)\cdot \boldsymbol{x})\boldsymbol{M}(\boldsymbol{x},t) - \frac{\boldsymbol{M}(\boldsymbol{x},t)}{T_2} - \nabla\cdot(D(\boldsymbol{x})\nabla \boldsymbol{M}). \tag{1}$$

This equation describes the time evolution of the complex-valued, transverse spin magnetization ($\boldsymbol{M}$) resulting from an externally applied, spatially and temporally varying magnetic field ($\boldsymbol{G}(t)\cdot\boldsymbol{x}$). Here i is the imaginary unit, γ is the gyromagnetic ratio of ^1H, $\boldsymbol{x}$ is the spin position vector, $\boldsymbol{G}(t)$ is the time-varying magnetic field gradient vector used to encode diffusion, T_2 is the transverse relaxation time, and $D(\boldsymbol{x})$ is the local diffusion coefficient. The dMRI signal is expressed by the following integral over the voxel volume (here REV),

$$S(t) = \int_V |\boldsymbol{M}(\boldsymbol{x},t)| d\boldsymbol{x}. \tag{2}$$

Diffusion-weighting results in attenuation of the signal, which is normalized by the non-diffusion-weighted signal, S_0, to provide an attenuation ratio, $E = S/S_0$. If the diffusion is Gaussian, then the signal attenuation can be modeled as $E = e^{-\boldsymbol{b}:\boldsymbol{D}}$ [14], where $\boldsymbol{D}$ is a second rank tensor that describes the apparent diffusion coefficients in the voxel [14], and $\boldsymbol{b}$ represents the cumulative magnetization effect of the applied diffusion gradients. A typical diffusion-encoding sequence consists of two gradients of strength and orientation $\boldsymbol{g}$, applied for duration δ, and separated by a

diffusion time Δ, which results in the relationship $\boldsymbol{b} = (\gamma \boldsymbol{g} \delta)^2 (\Delta - \delta/3)$ [14].

In complex tissues such as muscle, the apparent diffusion tensor is anisotropic and composed of three distinct eigenvalues (λ_1, λ_2, and λ_3), which correspond to the principal directions of $\boldsymbol{D}$. The eigenvalues are employed to define various dMRI metrics such as fractional anisotropy $\left(\mathrm{FA} = \sqrt{\frac{(\lambda_1-\lambda_2)^2+(\lambda_2-\lambda_3)^2+(\lambda_3-\lambda_1)^2}{2(\lambda_1^2+\lambda_2^2+\lambda_3^2)}}\right)$, mean diffusivity ($\mathrm{MD} = (\lambda_1 + \lambda_2 + \lambda_3)/3$), and radial diffusivity ($\mathrm{RD} = (\lambda_2 + \lambda_3)/2$). These metrics characterize the diffusion rate and tensor anisotropy within the voxel.

Pulse Sequence Parameterization

While more advanced sequences have been used to extract complex information from tissue [15–17], here we focus on two related dMRI pulse sequences, the Stejskal-Tanner pulsed-gradient spin echo (PGSE) sequence [18] and a simplified version of the simulated echo acquisition mode (STEAM) diffusion-weighted sequence. Although ubiquitous, the PGSE sequence is limited in the diffusion times it can examine due to the short T_2 of skeletal muscle. STEAM sequences accommodate longer diffusion times [19, 20], but also necessitate more complex simulation of the sequence because the magnetization does not remain solely in the transverse plane. Here we use a simplified version of the STEAM sequence that ignores relaxation effects [21]. If relaxation is ignored in the PGSE sequence, then it also reduces to this simplified STEAM sequence, so we refer to the latter as a generalized diffusion-weighted sequence. This generalized sequence allows a wider range of diffusion times, and is introduced here to examine the effect of longer diffusion times on the sensitivity analysis.

The effective gradient of both the PGSE and generalized diffusion-weighted sequences can be described by Figure 1a. The key difference is that our analysis of the PGSE sequence includes the effects of T_2 relaxation, while the generalized diffusion-weighted sequence is devoid of T_2 (and T_1) relaxation. Previous work has suggested that the gradient duration has a smaller effect on dMRI signal than diffusion time [22], so we focus here only on the effect of diffusion time (Δ) and b-value. The gradient duration is fixed at 10 ms for the PGSE sequence and at 5 ms for generalized diffusion-weighted sequence, while TE is defined as $\Delta + \delta$. For each simulation, the gradient strength is calculated from the prescribed b-value and diffusion time.

Muscle Tissue Model

To model the effect of skeletal muscle microstructure on the dMRI signal, it is first necessary to create a model with parameterized geometric features. Skeletal muscle has a hierarchical order. It exhibits short-range order with parallel, elongated myocytes, each surrounded by a semi-permeable membrane and embedded in an extracellular matrix. This organization allows the formulation of a simplified skeletal muscle model consisting of infinitely long, parallel cylinders

arranged in a periodic hexagonal array (Figure 1b). This periodic arrangement allows for a representative elemental volume (REV), as shown in Figure 1b. By restricting our computation to a single REV, we can economically parameterize the domain and consider how microstructural changes affect the dMRI signal. The hexagonal cross-section of the myocyte allows the achievement of high volume fractions. This investigation ignores heterogeneity of myocyte size [10] or shape within the voxel, and is the necessary first step towards quantifying the sensitivity to individual myocyte parameters before including more complicated features.

The tissue model in the REV is defined by seven parameters: intra- and extra-cellular diffusion coefficients, cell diameter, volume fraction, membrane permeability and intra- and extra-cellular T_2 relaxation times. Water diffusion in the intra- and extracellular domains is characterized by two homogeneous (effective) diffusion coefficients, D_{in} and D_{ex}, which is representative of the cumulative effects of sub-cellular restriction within each domain [23].

The present model produces isotropic transverse diffusion, however, muscle exhibits transversely anisotropic diffusion [23–25]. The cause of this radial anisotropy has not been conclusively identified, so this aspect is set aside for now. Analytical solutions for the dMRI signal in simplified geometrical domains are known [26, 27], and progress has been made on more complex geometries [28]. However, current analytical solutions of heterogeneous domains of embedded, tightly packed cells either do not account for the independent effect of the extracellular compartment [29, 30], or assume a long-time diffusion limit, which is not applicable in skeletal muscle dMRI [9, 31]. In order to account for both of these considerations, we resort to a numerical solution of the Bloch-Torrey equation.

Numerical Methods

The Bloch-Torrey equation is integrated using the lattice Boltzmann method (LBM) on a D3Q7 stencil. This stencil corresponds to three dimensions and seven lattice directions (speeds). Full details of the implementation are presented in [32], and only a rudimentary description is given below. LBM is a mesoscale numerical scheme, employed here to simulate transport of the complex-valued transverse magnetization on a discrete grid as $\boldsymbol{M}(\boldsymbol{x}, t) = \sum_{i=0}^{6} \boldsymbol{g}_i(\boldsymbol{x}, t)$, where $\boldsymbol{g}_i(\boldsymbol{x}, t)$ is the complex spin probability distribution function, representing the two components of the transverse magnetization vector. Using the Bhatnagar-Gross-Krook collision model with a single relaxation factor (τ), the evaluation of $\boldsymbol{g}_i$ is approximated by a diffusion step,

$$\boldsymbol{g}_i'(\boldsymbol{x} + \boldsymbol{e}_i \cdot \delta x, t) - \boldsymbol{g}_i(\boldsymbol{x}, t) = -\frac{1}{\tau}\left[\boldsymbol{g}_i(\boldsymbol{x}, t) - \boldsymbol{g}_i^{eq}(\boldsymbol{x}, t)\right], \tag{3}$$

followed by a reaction step,

$$g_i(\boldsymbol{x}, t + \delta t) = \exp\left(-\frac{\delta t}{T_2} - i\gamma G^n \boldsymbol{x}_i \delta t\right) g_i'(\boldsymbol{x}, t). \tag{4}$$

where δx and δt are the lattice spacing and time step respectively, and $\boldsymbol{e}_i$ represents the lattice speeds. Intra-domain boundary conditions handle the effect of spins crossing the membrane while modified periodic boundary conditions account for the non-periodic magnetization accumulation over the periodic geometry of the REV. Because the muscle tissue is modeled as a unidirectional composite with infinite cylindrical fibers in the axial direction, translational symmetry allows the use of a single node in that direction while retaining a three-dimensional treatment of the domain. Details of the numerical discretization parameters used to minimize numerical error of the simulation are given in Supporting Information Figure S1.

For each simulation, six gradient directions and a non-diffusion weighted acquisition are simulated [33], and the signal attenuation, $E(\boldsymbol{q})$, is computed. To account for the effect of noise, Rician noise is added to the signal for the PGSE sequence at single acquisition SNR levels of 10, 25 and 50 based on the non-diffusion weighted signal [8, 34]. This is done for multiple numbers of signal averages (NSA = 1, 5, 10, 15, and 20) with the average signal fit to a diffusion tensor using the fanDTasia ToolBox [35]. From the diffusion tensor, FA, MD, RD and the tensor eigenvalues (λ_1, λ_2, and λ_3) are calculated. The effect of noise was not considered for the generalized diffusion-weighted sequence.

Global Sensitivity Analysis

To determine how changes in microstructure and sequence parameters affect the dMRI signal, a global sensitivity analysis was performed, which characterizes how changes to the input parameters effect the variance of the model's output [36]. We use the method developed by Saltelli et al. [37, 38], as implemented in the open source SaLib python package [39]. Reviews of this method have been presented elsewhere [40, 41].

The analysis decomposes the variance of the model's output into the variances of the individual input parameters and the variances due to non-linear combinations of multiple parameters. The method computes first, second and total-order sensitivity indices of the input parameters. First-order sensitivity indices describe the fraction of the total variance of the output attributed to the variance of a particular parameter. For example, a first-order volume fraction sensitivity index of 0.50 for FA would mean that 50% of the total variance in FA can be described by variance in only the volume fraction. Second-order indices capture the response of the model to the combination of two parameters that cannot be written as a superposition of two first-order effects independently.

Total-order indices are the sum of first, second, and higher-order indices for each parameter. They describe the total contribution of a parameter to the variance of the system output. Parameters are sampled independently from a uniform distribution of values within a given range. The total number of model evaluations is 2N(p+1), where p is the number of parameters and N is the number of independent samples of each parameter.

Microstructural parameter ranges were extracted from reported literature values and are presented in Table 1 along with the examined ranges of the dMRI sequence parameters. Parameter sampling was preformed using a Sobol sequence, which is a quasi-random, low discrepancy method that allows more uniform coverage of the input parameter space than traditional Monte Carlo methods [37, 42]. For the PGSE sequence, nine parameters were examined and, 5,000 samples were taken for each parameter, resulting in a total of 100,000 parameter sets. For the generalized diffusion-weighted sequence, only seven parameters were considered, leading to 80,000 parameter sets. These parameter sets defined the microstructural REV and dMRI sequence for which the Bloch-Torrey equation was numerically solved. The resulting signals were used to calculate FA, MD, RD and the tensor eigenvalues. For both the PGSE and generalized diffusion-weighted sequences, a sensitivity analysis was performed for all six dMRI metrics at each of the prescribed SNR levels. Because the REV produces transversely isotropic diffusion, only radial diffusivity is reported instead of λ_2 and λ_3 because these results are all similar.

3 Results

The computations for the present sensitivity analysis were performed on the San Diego Supercomputing Center's Comet cluster [43], which consists of 1,944 nodes, each with 2 x 12 core processors (Intel Xeon E5-2680 v3 2.5 Ghz). 40 nodes were used with three simulations run simultaneously on each node and each simulation using eight cores. The simulations for the entire study took approximately 6000 core hours. The numerical solutions of equation 1 were post-processed to calculate the diffusion tensor and dMRI metrics. A sensitivity analysis was performed for each dMRI metric at each noise level.

The noise-free results of the sensitivity analysis of the PGSE sequence, along with the sensitivity indices for SNR levels of 10, 25, and 50, are presented in Figure 2. Figure 3 shows the cumulative L2-norm difference between the sensitivity indices with and without added noise ($\|\mathbf{Si}^{SNR} - \mathbf{Si}^{nf}\|$, where $\mathbf{Si}^{SNR}$ and $\mathbf{Si}^{nf}$ are vectors of the noise-added and noise-free sensitivity indices, respectively). It demonstrates the effect of SNR and signal averaging on the sensitivity indices. Finally, results of the sensitivity analysis for the generalized diffusion-weighted sequence are given in Figure 4. Complete results from the sensitivity analyses are available in Supporting Information Tables S1 and S2.

4 Discussion

Effect of synthetic noise

The goal of the present sensitivity study is to identify the effect of microstructural and sequence parameters on dMRI measurements. We begin our discussion by focusing on the results of the sensitivity analysis for the PGSE pulse sequence. The effect synthetic noise has on the sensitivity indices is determined by comparing the effect of three different noise levels, SNR=10, 25 and 50.

Focusing on the first-order indices, Figure 2a indicates that the strongest effect of adding noise is a decrease in the sensitivity of MD and λ_1 to the intracellular diffusion coefficient, and a decrease in the sensitivity of FA and RD to fiber diameter. A comparison of sensitivity indices for different SNR levels shows that lower SNR leads to a decrease in first-order sensitivity for a majority of the microstructural parameters. Considering only noise-free indices larger than 0.10, there is an average decrease of 51.4%, 17.8% and 6.5% for SNR levels of 10, 25 and 50, respectively. This means that for low SNR levels, the measured signal will be less sensitive to changes in the underlying microstructure.

Turning to the total-order indices shown in Figure 2b, we see that for low SNR, the total order sensitivity of the model is inflated for all parameters because the random perturbations from noise are artificially assigned to higher order effects. These results illustrate the importance of requiring high SNR in order to connect skeletal muscle dMRI metrics to the underlying tissue microstructure. For low SNR, the dMRI signal will be more influenced by noise than changes in the microstructure, particularly for microstructural parameters associated with weak sensitivity indices, such as permeability and the extracellular diffusion coefficient.

For microstructural parameters that have low or no effect on dMRI metrics, such as T_2 or b-value, the effect of noise is consistent for each dMRI metric, suggesting that one can use the increase in the total-order sensitivity to these parameters as a metric for the effect of system noise. Under this interpretation, for an SNR of 10, noise appears to account for approximately 40% of the variance of the dMRI metrics, while for an SNR of 25 the noise accounts for approximately 10%. For all SNR levels, FA is much more strongly affected by noise than the MD, RD of λ_1. When this system noise metric is larger than the noise-free total-order index of a particular microstructural parameter, then noise has a larger effect on the measured signal than the parameter in question. As such, the dMRI signal cannot be directly related to that parameter. Thus comparing total-order indices with the effect of system noise can be a useful method of determining when the SNR is high enough that a microstructural parameter (in particular, volume fraction and permeability) can be related to the dMRI signal.

Figure 3 examines how SNR and NSA affect the first-order sensitivity indices relative to the

noise-free indices. The L2-norm of the difference is used as a measure of the effect of noise on the sensitivity of the system as a whole. As expected, the results indicate that the accuracy in estimating sensitivity indices increases with NSA and SNR. Increasing the number of acquisitions increases SNR by a factor of $\sqrt{\text{NSA}}$. For increasing SNR, the order of convergence of the first-order sensitivity indices to the noise-free indices is approximately 1.5, indicating that even small increases in SNR can improve the ability to resolve the sensitivity of the dMRI metrics to the underlying microstructure. Previous authors have commented on the necessary SNR thresholds in skeletal muscle dMRI and suggested minimum SNR levels of 40-60 [8], although lower SNR levels are often reported in practice [44–46]. In order for dMRI to be sensitive to changes in the microstructure, our results suggest that an SNR threshold of 50 be achieved, likely requiring increased NSA [46].

Microstructural Parameters

Next, we consider the sensitivity indices of the microstructural parameters. The intracellular diffusion coefficient has the largest first-order effect on all dMRI parameters except FA, which is most sensitive to diameter. Because of the high volume fractions considered, the intracellular domain occupies most of the REV, so it is unsurprising that this diffusion coefficient strongly affects the apparent diffusion tensor.

After the intracellular diffusion coefficient, the second most sensitive microstructural parameter is the cell diameter. Changing fiber diameter strongly effects metrics associated with radial diffusion (FA, RD) and not axial diffusion (λ_1). The effect of cell diameter on radial diffusion has been illustrated previously [19, 47], and along with current results, this bolsters the claim that fiber diameter can be inferred from the dMRI signal. The third most sensitive microstructural parameter is the extracellular diffusion coefficient. Its effect across dMRI parameters is similar to that of the intracellular diffusion coefficient but to a lesser extent. This is because the extracellular domain has a smaller volume fraction than the intracellular domain, so the associated parameters contribute less to the overall signal. However, this contribution is partially boosted by the extracellular domain having a higher T_2 than the intracellular domain. The final microstructural parameter that has a notable first-order effect is permeability. The effect of permeability is most pronounced on FA and RD. Two microstructural parameters that have little influence on the calculated dMRI metrics are the T_2 relaxation values (within the considered T_2 ranges). Although relatively unimportant, the largest second-order indices are associated with the effects of diameter and intracellular diffusion coefficient on FA and RD (see Supporting Information Tables S1 and S2 for full second-order results).

PGSE pulse sequence sensitivity

Turning to the PGSE pulse parameters in Figure 2, FA and RD are slightly sensitive to diffusion time, while λ_1 is insensitive to diffusion time. This insensitivity of λ_1 to diffusion time is characteristic of tissue with parallel myofibers [48]. In more complex muscle tissue experiments [6], λ_1 exhibits a small but noticeable dependence on diffusion time, ostensibly associated with additional longitudinal barriers or dispersion of the fiber orientation that are not present in our simplified REV model. In the radial direction, diffusion is restricted due to the finite permeability of cell membranes. As the diffusion time increases, more interior spins interact with these membranes, leading to sensitivity to increased diffusion time. For a constant diffusion time, the model is not sensitive to changes in b-value over the examined range.

Generalized diffusion-weighted pulse sequence sensitivity

We next examine the sensitivity indices of the generalized diffusion-weighted sequence. The diffusion time dependence of the dMRI signal in skeletal muscle is well established [20, 48], and measuring skeletal muscle dMRI over a range of diffusion times is an active area of research. Analyzing the generalized diffusion-weighted sequence allows investigation of how the sensitivity of the dMRI model changes as the diffusion time increases. The results, shown in Figure 4, are generally similar to the results of the PGSE sequence, with sensitivity to the intracellular diffusion coefficient and diameter being the most prominent. Additionally, it is noted that the effect of permeability is increased while that of the extracellular diffusion coefficient is decreased.

The sensitivity to the b-value is zero, but the effect of diffusion time, although still a weak effect compared to that of microstructural parameters, is stronger than it was for the PGSE sensitivity study. Previous results have shown a b-value dependence of the diffusion tensor eigenvalues [25]. However, in those results, the b-value was varied by changing TE, which in turn often corresponds to varying the diffusion time. The b-value insensitivity reported here is attributed to insensitivity to the gradient strength, since it was the latter that was actually varied to match the sampled b-value. Additionally, the model's insensitivity to the b-value does not account for errors in estimating the diffusion tensor, which has been shown to depend on the b-value (and number of gradient directions) as well [8, 25]. These results illustrate that caution needs to be exercised when comparing reported muscle dMRI metrics; differences in both b-value and TE (and its relationship to diffusion time) need to be considered, even for PGSE sequences.

Our generalized diffusion-weighted sequence is a simplified version of STEAM and further work is required to fully analyze the sensitivity of STEAM to T_2 and T_1 relaxation, as well as the effects of flip angle and pulse timing. Our results suggest that the overall sensitivity of dMRI metrics is similar for a broad range of diffusion times, but that the sensitivity of certain parameters,

such as permeability, is increased for longer diffusion times.

Comment on parameter ranges

An important consideration when interpreting global sensitivity indices is the effect of the independent parameter ranges considered. These sensitivity indices only examine how the dMRI metrics are affected by changes within the examined range. Although the model was not found to be very sensitive to volume fractions, this is probably related to setting the volume range to 0.70 to 0.95, which is a reasonable range for muscle fibers. Additionally, the ranges of diffusion coefficients considered are the same for both extracellular and intracellular domains. While preliminary evidence suggests that the extracellular domain may have a larger diffusion coefficient [49], this evidence is inconclusive. If the ranges of the two diffusion coefficients were different, then changes in volume fraction would be expected to have a larger effect on the signal. An illustration of how changes in the parameter range affects sensitivity indices is provided in Supporting Information Table S3.

Recall that different T_2 ranges were considered for the two domains, which is consistent with the suggestion that the extracellular domain has a higher T_2 than the intracellular domain [50]. Because of the higher extracellular T_2, the extracellular compartment signal will decay more slowly, providing a larger contribution to the overall signal for long TE. This will likely increase the sensitivity to parameters associated with the extracellular domain [11, 51]. Even though the sensitivity analysis does not reveal high sensitivity to T_2, the difference in the intra- and extracellular T_2 ranges creates the above effect, illustrating that this difference should be accounted for when modeling muscle dMRI. This T_2 difference influences the signal behavior as permeability increases [9, 52], and given the T_2 ranges, it is not possible to factor out this effect. Our results show that variations within the examined ranges do not substantially affect any of the dMRI metrics, however, further work is needed to better understand the effect of T_2 compartmentalization on skeletal muscle dMRI.

Comparison with prior studies

Comparing the present sensitivity analysis results with those reported by prior studies, we note a number of similarities and differences. Hall and Clark [10] and Berry et al. [11] did not examine the role of the diffusion coefficient, and Bates et al. [12] kept both intra- and extracellular diffusion coefficients the same. Our results suggest that both intra- and extracellular effective diffusion coefficients have an effect on dMRI signal. Although some tissue models of muscle dMRI only use a single diffusion coefficient to represent the entire muscle [10, 12, 19, 53], this is not justified by the differences in the histoarchitectures of the intra- and extracellular domains. The extracellular space consists of a hierarchical collagen fiber matrix, while the intracellular space

is composed of a more organized protein based matrix. MR-based experimental evidence suggests that muscle consists of separate pools with different diffusion coefficients [49, 54–56]. Our results indicate that both coefficients substantially affect the signal. Further investigation is needed to determine how different these effective diffusion coefficients are and if it is appropriate to treat them as a single coefficient. The putative effect of subcellular structures on the effective diffusion coefficients points to limitations of the adopted simplified structural model of muscle, especially in modeling axial diffusion. Improved tissue models should incorporate the effect of subcellular parameters such as sarcomere length [6] or myofibril distribution [10] on the determination of effective diffusion coefficients.

The differences between prior and the present results extend to permeability and diameter as well. These were considered by Hall and Clark [57] and Berry et al. [11] but with disparate results. Hall and Clark examined the change in entropy of the dMRI signal and found that permeability has the largest effect on this measure. In contrast, Berry et al. found that fiber diameter has a larger effect. Our results agree with those of Berry et al, although we find that fiber diameter has a stronger relative effect compared to permeability. A caveat in comparing these studies concerns the tissue model adopted. Hall and Clark used a hierarchical tissue model of muscle consisting of cylinders embedded in larger cylinders and also considered an impermeable baseline case. These embedded cylinders are more representative of myofibrils than myocytes. As such, the change in permeability of these embedded cylinders compares more directly to a change in our model's effective intracellular diffusion coefficient, in which case our results agree with theirs. Berry et al. modify the permeability of the myocytes by randomly deleting the cell wall of a portion of the cells in the domain. This can be contrasted to our use of a finite permeability membrane on all cells and may explain the differences in results. Our model accounts for finite water permeability by imposing an interfacial flux condition [32]. This closely relates to permeability changes related to changes in muscle metabolism [6]. Additionally, damage found in dystrophin-deficient muscle [4, 5] is thought to lead to mechanically-induced tears in the membrane, which can also be modeled as an increase in the average flux across the membrane. Bates et al. [12] model permeability in this way as well, but they do not systematically examine its effect.

Another key difference with previous studies is our treatment of pulse parameters. Berry et al. examine a single diffusion time and gradient strength. Bates et al. consider these parameters individually, although their sensitivity analysis is performed at a single diffusion time and gradient strength. Hall and Clark examine the effect of diffusion time and gradient strength but use them as fixed parameters in their study. In contrast, we examined diffusion time and b-value as input

parameters to the sensitivity analysis.

The present sensitivity analysis, as a whole, agrees most closely with Berry et al. and Bates et al., but not with Hall and Clark, likely due to the tissue model differences mentioned above. Our general agreement with Berry et al. and Bates et al. is notable; they both perform their analysis using relatively short diffusion times (9 and 7 ms respectively) while we consider a much larger range of diffusion times and b-values. This similarity suggests that the relative influence of individual parameters is consistent across a range of diffusion times and b-values. A point further supported by the agreement between the PGSE and generalized diffusion-weighted sequence results.

Usefulness of sensitivity indices

Sensitivity indices are only meaningful if the parameter ranges are realistic. These sensitivity indices are global indices and describe the effect over the prescribed range as a whole. The parameter ranges chosen here are intentionally broad to include the majority of values reported in the literature. This choice most likely affects the sensitivity analysis results. In particular, the strong effect of the intracellular diffusion coefficient may be partly due to the wide parameter range used. Nevertheless, the results presented here not only isolate the microstructural parameters that have the strongest effect on the dMRI signal, but also point out which ones future investigations should focus on measuring. Additional measurements will allow refining the normal and pathological range of these parameters, thus leading to more accurate sensitivity indices.

With this proviso, the results presented here can still help estimate relative importance of candidate microstructural parameters in interpreting the dMRI signal. For example, if one wishes to measure permeability, the intracellular coefficient and diameter must be accurately estimated, since a small change in either of them could easily overwhelm any change in permeability. Another possible use of these results is in making comparisons between dMRI metrics. As an example, if an experiment shows a difference in MD but not in FA (like that reported between athletes and non-athletes [58]), then this is unlikely to be caused by changes in diameter or permeability, as both of these have higher sensitivity to FA than MD. Rather, intra- and extracellular diffusion coefficients are better candidates to explain such a difference, as they have a small impact on FA but a larger impact on MD. This argument does not conclusively attribute dMRI change to a certain microstructural parameter, but it does help identify candidates, and rule out others, for further investigation. Finally, the present methodology can be used to optimize dMRI sequence development by maximizing the sensitivity of the signal to the chosen microstructural parameters.

5 Conclusion

The goal of this study is to determine which microstructural and pulse parameters most influence muscle dMRI signal. We performed a global sensitivity analysis of the effect that microstructural and PGSE pulse parameters have on dMRI metrics of FA, MD, RD and the diffusion tensor eigenvalues, as well as an analysis of a generalized diffusion-weighted sequence, which allowed us to examine a larger range of diffusion times. We also examined the effect that adding synthetic noise has on the sensitivity indices. We concluded that SNR levels of at least 50 should be attained to accurately interpret dMRI in terms of the underlying microstructure. Increasing NSA is an appropriate method of attaining this higher SNR.

We report that among the examined microstructural parameters the intracellular diffusion coefficient has the strongest effect and that cell diameter is more influential than permeability in the transverse direction. We found that both the PGSE and generalized diffusion-weighted sequences had similar sensitivity to microstructural parameters. Although our results indicate that the dMRI metrics are not sensitive to T_2 variations, we do not infer that the difference between intra- and extracellular T_2 values should be ignored. By identifying the key microstructural features that affect dMRI measurements, the present sensitivity results can help interpret dMRI signal measurements and inform further model development by reducing the number of microstructural parameters considered.

Acknowledgments

The computations reported in this work used the Extreme Science and Engineering Discovery Environment (XSEDE), which is supported by NSF grant ACI-1548562. Additional support was provided by an NSF GRFP award to N. Naughton, the R.A. Pritzker endowed chair, and NSF grants CBET-1236451 and CMI-1762774. The contributions of two anonymous reviewers in improving this manuscript is also gratefully acknowledged.

References

[1] Mann CJ, Perdiguero E, Kharraz Y, Aguilar S, Pessina P, Serrano AL, et al. Aberrant repair and fibrosis development in skeletal muscle. Skeletal Muscle 2011;1(1):21.

[2] Kirkendall DT, Garrett WE. The effects of aging and training on skeletal muscle. The American Journal of Sports Medicine 1998;26(4):598–602.

[3] Tieland M, Trouwborst I, Clark BC. Skeletal muscle performance and ageing. Journal of Cachexia, Sarcopenia and Muscle 2018;9(1):3–19.

[4] Brussee V, Tardif F, Tremblay JP. Muscle fibers of mdx mice are more vulnerable to exercise than those of normal mice. Neuromuscular Disorders 1997;7(8):487–492.

[5] Petrof BJ, Shrager JB, Stedman HH, Kelly AM, Sweeney HL. Dystrophin protects the sarcolemma from stresses developed during muscle contraction. Proceedings of the National Academy of Sciences 1993;90(8):3710–3714.

[6] Winters KV, Reynaud O, Novikov DS, Fieremans E, Kim SG. Quantifying myofiber integrity using diffusion MRI and random permeable barrier modeling in skeletal muscle growth and Duchenne muscular dystrophy model in mice. Magnetic Resonance in Medicine 2018;http://doi.wiley.com/10.1002/mrm.27188.

[7] Jelescu IO, Budde MD. Design and validation of diffusion MRI models of white matter. Frontiers in Physics 2017;5:61.

[8] Damon BM. Effects of image noise in muscle diffusion tensor (DT)-MRI assessed using numerical simulations. Magnetic Resonance in Medicine 2008;60(4):934–944. http://doi.wiley.com/10.1002/mrm.21707.

[9] Naughton NM, Georgiadis JG. Comparison of two-compartment exchange and continuum models of dMRI in skeletal muscle. Physics in Medicine & Biology 2019;64(15):155004.

[10] Hall MG, Clark CA. Diffusion in hierarchical systems: A simulation study in models of healthy and diseased muscle tissue. Magnetic Resonance in Medicine 2017;78(3):1187–1198. http://doi.wiley.com/10.1002/mrm.26469.

[11] Berry DB, Regner B, Galinsky V, Ward SR, Frank LR. Relationships between tissue microstructure and the diffusion tensor in simulated skeletal muscle. Magnetic Resonance in Medicine 2018;80(1):317–329. http://doi.wiley.com/10.1002/mrm.26993.

[12] Bates J, Teh I, McClymont D, Kohl P, Schneider JE, Grau V. Monte Carlo Simulations of Diffusion Weighted MRI in Myocardium: Validation and Sensitivity Analysis. IEEE Transactions on Medical Imaging 2017;36(6):1316–1325. http://ieeexplore.ieee.org/document/7875442/.

[13] Torrey HC. Bloch equations with diffusion terms. Physical Review 1956;104(3):563.

[14] Basser PJ. Relationships between diffusion tensor and q-space MRI. Magnetic Resonance in Medicine 2002;47(2):392–397.

[15] Nilsson M, Lasič S, Drobnjak I, Topgaard D, Westin CF. Resolution limit of cylinder diameter estimation by diffusion MRI: The impact of gradient waveform and orientation dispersion. NMR in Biomedicine 2017;30(7):e3711. http://doi.wiley.com/10.1002/nbm.3711.

[16] Mitra PP. Multiple wave-vector extensions of the NMR pulsed-field-gradient spin-echo diffusion measurement. Physical Review B 1995;51(21). https://journals.aps.org/prb/pdf/10.1103/PhysRevB.51.15074.

[17] Drobnjak I, Siow B, Alexander DC. Optimizing gradient waveforms for microstructure sensitivity in diffusion-weighted MR. Journal of Magnetic Resonance 2010;206(1):41–51.

[18] Stejskal EO, Tanner JE. Spin diffusion measurements: spin echoes in the presence of a time-dependent field gradient. The Journal of Chemical Physics 1965;42(1):288–292.

[19] Fieremans E, Lemberskiy G, Veraart J, Sigmund EE, Gyftopoulos S, Novikov DS. In vivo measurement of membrane permeability and myofiber size in human muscle using time-dependent diffusion tensor imaging and the random permeable barrier model. NMR in Biomedicine 2017;30(3).

[20] Sigmund EE, Novikov DS, Sui D, Ukpebor O, Baete S, Babb JS, et al. Time-dependent diffusion in skeletal muscle with the random permeable barrier model (RPBM): application to normal

controls and chronic exertional compartment syndrome patients. NMR in Biomedicine 2014;27(5):519–528.

[21] Rose JN, Nielles-Vallespin S, Ferreira PF, Firmin DN, Scott AD, Doorly DJ. Novel insights into in-vivo diffusion tensor cardiovascular magnetic resonance using computational modeling and a histology-based virtual microstructure. Magnetic Resonance in Medicine 2019;81(4):2759–2773.

[22] Baxter GT, Frank LR. A computational model for diffusion weighted imaging of myelinated white matter. Neuroimage 2013;75:204–212.

[23] Galban CJ, Maderwald S, Uffmann K, de Greiff A, Ladd ME. Diffusive sensitivity to muscle architecture: a magnetic resonance diffusion tensor imaging study of the human calf. European Journal of Applied Physiology 2004;93(3):253–262.

[24] Karampinos DC, King KF, Sutton BP, Georgiadis JG. Myofiber ellipticity as an explanation for transverse asymmetry of skeletal muscle diffusion MRI in vivo signal. Annals of Biomedical Engineering 2009;37(12):2532–2546.

[25] Froeling M, Nederveen AJ, Nicolay K, Strijkers GJ. DTI of human skeletal muscle: The effects of diffusion encoding parameters, signal-to-noise ratio and T2 on tensor indices and fiber tracts. NMR in Biomedicine 2013;26(11):1339–1352. http://doi.wiley.com/10.1002/nbm.2959.

[26] Tanner JE, Stejskal EO. Restricted self-diffusion of protons in colloidal systems by the pulsed-gradient, spin-echo method. The Journal of Chemical Physics 1968;49(4):1768–1777.

[27] Söderman O, Jönsson B. Restricted diffusion in cylindrical geometry. Journal of Magnetic Resonance, Series A 1995;117(1):94–97.

[28] Grebenkov DS. Pulsed-gradient spin-echo monitoring of restricted diffusion in multilayered structures. Journal of Magnetic Resonance 2010;205(2):181–195.

[29] Novikov DS, Fieremans E, Jensen JH, Helpern JA. Characterizing microstructure of living tissues with time-dependent diffusion. Proceedings of the National Academy of Sciences 2012;111(14):5088–5093. http://arxiv.org/abs/1210.3014{%}0Ahttp://dx.doi.org/10.1073/pnas.1316944111.

[30] Fieremans E, Lemberskiy G, Veraart J, Sigmund EE, Gyftopoulos S, Novikov DS. In vivo measurement of membrane permeability and myofiber size in human muscle using time-dependent diffusion tensor imaging and the random permeable barrier model. NMR in Biomedicine 2017;30(3):e3612. http://doi.wiley.com/10.1002/nbm.3612.

[31] Sen PN, Basser PJ. A model for diffusion in white matter in the brain. Biophysical Journal 2005;89(5):2927–2938.

[32] Naughton NM, Tennyson CG, Georgiadis JG. Lattice Boltzmann method for simulation of diffusion magnetic resonance imaging physics in heterogeneous tissue models. arXiv preprint arXiv:190700908 2019;.

[33] Hasan KM, Parker DL, Alexander AL. Comparison of gradient encoding schemes for diffusion-tensor MRI. Journal of Magnetic Resonance Imaging 2001;13(5):769–780.

[34] Gudbjartsson H, Patz S. The Rician distribution of noisy MRI data. Magnetic Resonance in

Medicine 1995;34(6):910–914.

[35] Barmpoutis A, Vemuri BC. A unified framework for estimating diffusion tensors of any order with symmetric positive-definite constraints. In: Biomedical Imaging: From Nano to Macro, 2010 IEEE International Symposium on IEEE; 2010. p. 1385–1388.

[36] Sobol IM. Global sensitivity indices for nonlinear mathematical models and their Monte Carlo estimates. Mathematics and Computers in Simulation 2001;55(1-3):271–280.

[37] Saltelli A. Making best use of model evaluations to compute sensitivity indices. Computer Physics Communications 2002;145(2):280–297.

[38] Saltelli A, Annoni P, Azzini I, Campolongo F, Ratto M, Tarantola S. Variance based sensitivity analysis of model output. Design and estimator for the total sensitivity index. Computer Physics Communications 2010;181(2):259–270.

[39] Herman J, Usher W. SALib: an open-source Python library for sensitivity analysis. The Journal of Open Source Software 2017;2(9).

[40] Saltelli A, Ratto M, Andres T, Campolongo F, Cariboni J, Gatelli D, et al. Global sensitivity analysis: the primer. John Wiley & Sons; 2008.

[41] Zhang XY, Trame M, Lesko L, Schmidt S. Sobol sensitivity analysis: a tool to guide the development and evaluation of systems pharmacology models. CPT: Pharmacometrics & Systems Pharmacology 2015;4(2):69–79.

[42] Sobol' IM. On the distribution of points in a cube and the approximate evaluation of integrals. Zhurnal Vychislitel'noi Matematiki i Matematicheskoi Fiziki 1967;7(4):784–802.

[43] Towns J, Cockerill T, Dahan M, Foster I, Gaither K, Grimshaw A, et al. XSEDE: Accelerating Scientific Discovery. Computing in Science & Engineering 2014;16(5):62–74. doi.ieeecomputersociety.org/10.1109/MCSE.2014.80.

[44] Hata J, Yagi K, Hikishima K, Numano T, Goto M, Yano K. Characteristics of diffusion-weighted stimulated echo pulse sequence in human skeletal muscle. Radiological physics and technology 2013;6(1):92–97.

[45] Hooijmans M, Damon B, Froeling M, Versluis M, Burakiewicz J, Verschuuren J, et al. Evaluation of skeletal muscle DTI in patients with duchenne muscular dystrophy. NMR in Biomedicine 2015;28(11):1589–1597.

[46] Rockel C, Noseworthy MD. An exploration of diffusion tensor eigenvector variability within human calf muscles. Journal of Magnetic Resonance Imaging 2016;43(1):190–202.

[47] Li H, Jiang X, Xie J, McIntyre JO, Gore JC, Xu J. Time-dependent influence of cell membrane permeability on MR diffusion measurements. Magnetic Resonance in Medicine 2016;75(5):1927–1934.

[48] Kim S, Chi-Fishman G, Barnett AS, Pierpaoli C. Dependence on diffusion time of apparent diffusion tensor of ex vivo calf tongue and heart. Magnetic Resonance in Medicine 2005;54(6):1387–1396. https://onlinelibrary.wiley.com/doi/pdf/10.1002/mrm.20676.

[49] Helmer KG, Seland JG, Henninger N, Sotak CH. Separation of the Intra- and Extracellular Apparent Diffusion Coefficients (ADC) of Water in Rat Skeletal Muscle using Spectroscopic

MEMRI. In: Proceedings of the 14th Annual Meeting of the International Society for Magnetic Resonance in Medicine;. .

[50] Cole WC, Leblanc AD, Jhingran SG. The origin of biexponential T2 relaxation in muscle water. Magnetic resonance in medicine 1993;29(1):19–24.

[51] Heemskerk AM, Damon BM. Diffusion Tensor MRI Assessment of Skeletal Muscle Architecture. Current Medical Imaging Reviews 2007;3(3):152–160.

[52] Harkins KD, Galons JP, Secomb TW, Trouard TP. Assessment of the effects of cellular tissue properties on ADC measurements by numerical simulation of water diffusion. Magnetic Resonance in Medicine 2009;62(6):1414–1422.

[53] Galbán CJ, Maderwald S, Uffmann K, de Greiff A, Ladd ME. Diffusive sensitivity to muscle architecture: a magnetic resonance diffusion tensor imaging study of the human calf. European Journal of Applied Physiology 2004;93(3):253–262. http://link.springer.com/10.1007/s00421-004-1186-2.

[54] Seland JG, Bruvold M, Anthonsen H, Brurok H, Nordhøy W, Jynge P, et al. Determination of water compartments in rat myocardium using combined D–T1 and T1–T2 experiments. Magnetic Resonance Imaging 2005;23(2):353–354.

[55] Ababneh Z, Beloeil H, Berde CB, Gambarota G, Maier SE, Mulkern RV. Biexponential parameterization of diffusion and T2 relaxation decay curves in a rat muscle edema model: decay curve components and water compartments. Magnetic Resonance in Medicine 2005;54(3):524–531.

[56] Morvan D. In vivo measurement of diffusion and pseudo-diffusion in skeletal muscle at rest and after exercise. Magnetic Resonance Imaging 1995;13(2):193–199.

[57] Hall MG, Clark CA. Diffusion in hierarchical systems: A simulation study in models of healthy and diseased muscle tissue. Magnetic Resonance in Medicine 2017;78(3):1187–1198.

[58] Okamoto Y, Kemp GJ, Isobe T, Sato E, Hirano Y, Shoda J, et al. Changes in diffusion tensor imaging (DTI) eigenvalues of skeletal muscle due to hybrid exercise training. Magnetic Resonance Imaging 2014;32(10):1297–1300.

[59] Bolsterlee B, D'Souza A, Gandevia SC, Herbert RD. How does passive lengthening change the architecture of the human medial gastrocnemius muscle? Journal of Applied Physiology 2017;122(4):727–738. http://jap.physiology.org/lookup/doi/10.1152/japplphysiol.00976.2016.

[60] Polgar J, Johnson MA, Weightman D, Appleton D. Data on fibre size in thirty-six human muscles: An autopsy study. Journal of the Neurological Sciences 1973;19(3):307–318. https://www.sciencedirect.com/science/article/pii/0022510X73900944?via{%}3Dihub.

[61] Aliev MK, Tikhonov AN. Obstructed metabolite diffusion within skeletal muscle cells in silico. Molecular and Cellular Biochemistry 2011;358(1-2):105–119.

[62] Porcari P, Hall MG, Clark CA, Greally E, Straub V, Blamire AM. The effects of ageing on mouse muscle microstructure: a comparative study of time-dependent diffusion MRI and histological assessment. NMR in Biomedicine 2018;31(3):e3881. http://doi.wiley.com/10.1002/nbm.3881.

[63] Sigmund EE, Novikov DS, Sui D, Ukpebor O, Baete S, Babb JS, et al. Time-dependent diffusion in skeletal muscle with the random permeable barrier model (RPBM): Application to normal controls and chronic exertional compartment syndrome patients. NMR in Biomedicine 2014;27(5):519–528. http://doi.wiley.com/10.1002/nbm.3087.

[64] Maier F, Bornemann A. Comparison of the muscle fiber diameter and satellite cell frequency in human muscle biopsies. Muscle & Nerve: Official Journal of the American Association of Electrodiagnostic Medicine 1999;22(5):578–583.

[65] Vincensini D, Dedieu V, Renou J, Otal P, Joffre F. Measurements of extracellular volume fraction and capillary permeability in tissues using dynamic spin-lattice relaxometry: studies in rabbit muscles. Magnetic Resonance Imaging 2003;21(2):85–93.

[66] Tanner JE. Transient diffusion in a system partitioned by permeable barriers. Application to NMR measurements with a pulsed field gradient. The Journal of Chemical Physics 1978;69(4):1748–1754.

[67] Landis CS, Li X, Telang FW, Molina PE, Palyka I, Vetek G. Equilibrium transcytolemmal water-exchange kinetics in skeletal muscle in vivo. Magnetic Resonance in Medicine 1999;42(3):467–478.

[68] Saab G, Thompson RT, Marsh GD. Multicomponent T2 relaxation of in vivo skeletal muscle. Magnetic Resonance in Medicine 1999;42(1):150–157.

[69] Fan RH, Does MD. Compartmental relaxation and diffusion tensor imaging measurements in vivo in λ-carrageenan-induced edema in rat skeletal muscle. NMR in Biomedicine 2008;21(6):566–573. http://doi.wiley.com/10.1002/nbm.1226.

[70] Crémillieux Y, Ding S, Dunn JF. High-resolution in vivo measurements of transverse relaxation times in rats at 7 Tesla. Magnetic Resonance in Medicine 1998;39(2):285–290.

[71] Saupe N, White LM, Stainsby J, Tomlinson G, Sussman MS. Diffusion tensor imaging and fiber tractography of skeletal muscle: optimization of B value for imaging at 1.5 T. American Journal of Roentgenology 2009;192(6):W282–W290.

[72] Oudeman J, Nederveen AJ, Strijkers GJ, Maas M, Luijten PR, Froeling M. Techniques and applications of skeletal muscle diffusion tensor imaging: a review. Journal of Magnetic Resonance Imaging 2016;43(4):773–788.

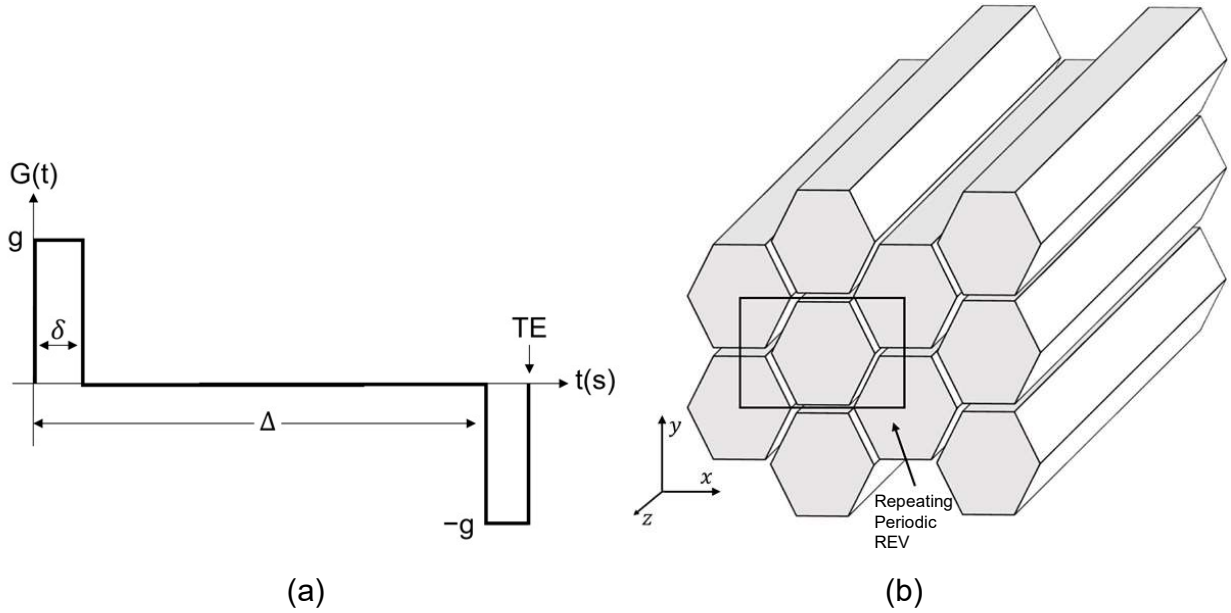

Figure 1: (a) Effective dMRI sequence and (b) periodic muscle fiber model. Solid rectangle designates the cross-section of the representative elementary volume (REV) in the x-y plane.

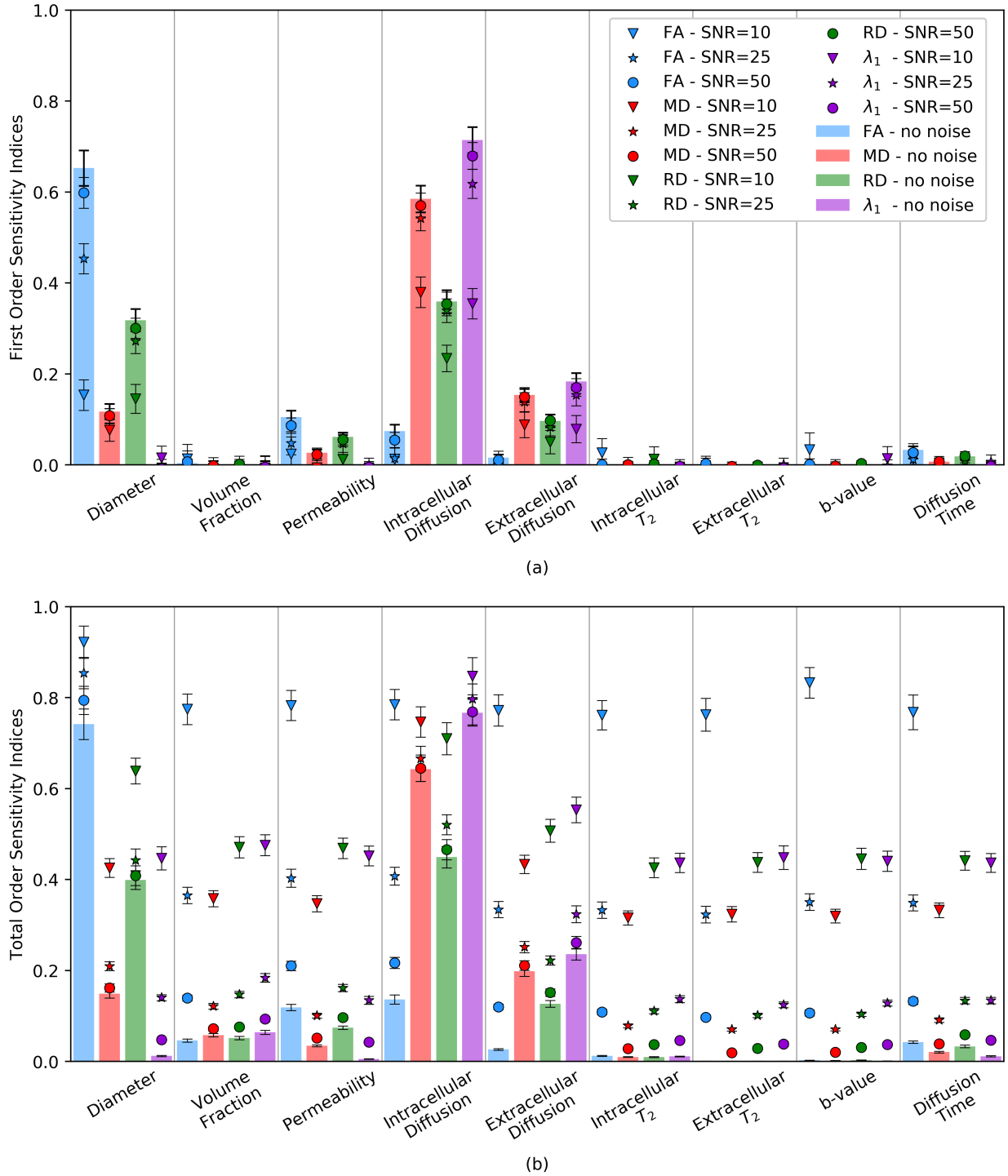

Figure 2: (a) First-order indices and (b) total-order indices for dMRI signal simulations with no added noise (color bars) and with added SNR levels of 10 (▽), 25 (⋆), 50 (o) and NSA = 1. Error bars are confidence intervals.

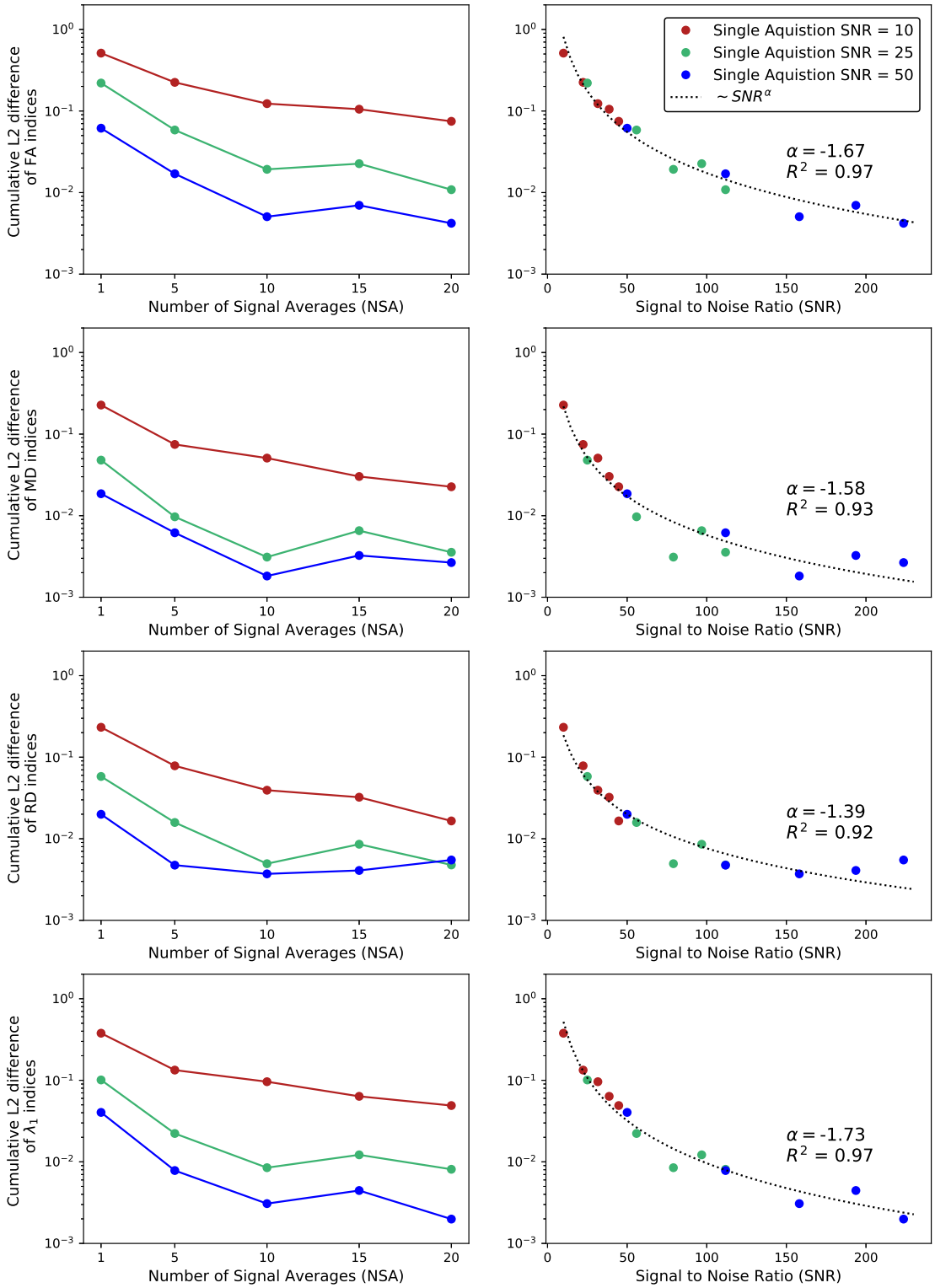

Figure 3: Sum of L2-norm difference between the first-order sensitivity indices for the noise-free results and when synthetic noise is added for different NSA (left panels) and SNR levels (right panels). Colors denote the SNR level for a single acquisition. The dotted lines in the right panels are power law regressions ($\sim SNR^{\alpha}$) and R^2 is the correlation coefficient.

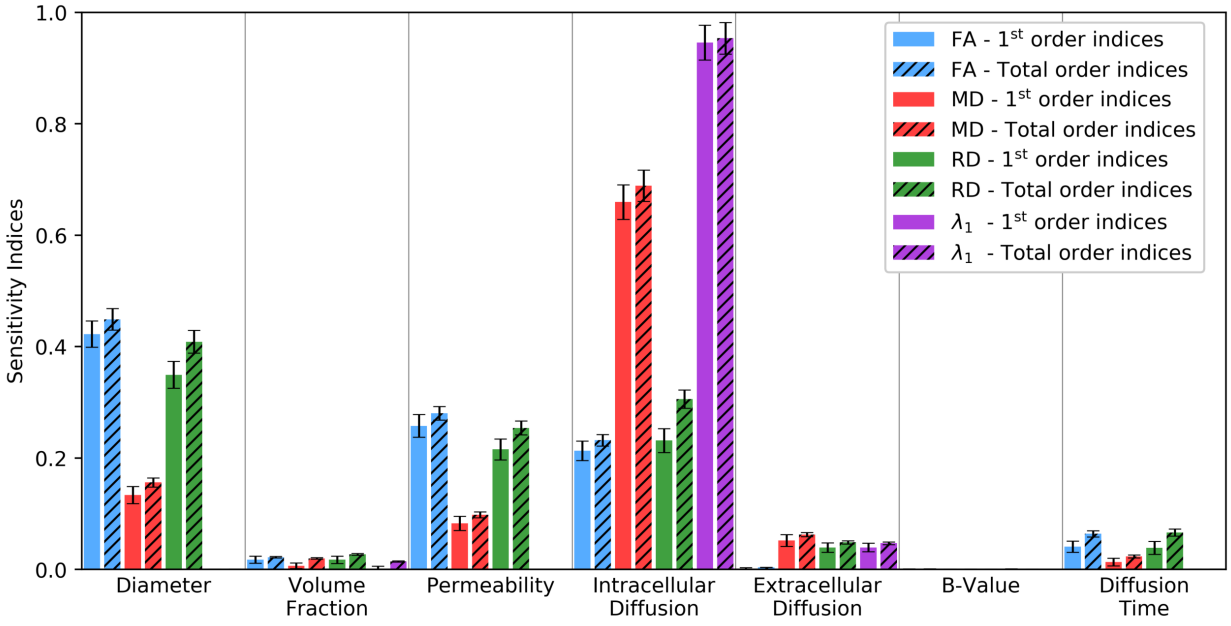

Figure 4: First and total-order indices for dMRI signal simulations of the generalized diffusion–weighted pulse sequence. Error bars are confidence intervals.

Table 1: Range of input parameters used in sensitivity study for both PGSE and the generalized diffusion sequence; parameters span range of experimentally observed values. * denotes parameters used in the sensitivity analysis of the PGSE sequence while † denotes parameters used in the analysis of the generalized diffusion-weighted sequence. T_2 ranges include reported values for field strengths between 0.5 - 7T.

Parameter	**Range**			**References**	
Myocyte Diameter	10	- 80	μm	[30, 59–64]	*†
Myocyte Volume Fraction	0.70	- 0.95		[56, 62, 65]	*†
Sarcolemma Membrane Permeability	10	- 100	$\mu m/s$	[30, 63, 66, 67]	*†
Intracellular Diffusion Coefficient	0.5	- 2.5	$\mu m^2/ms$	[49, 54–56]	*†
Extracellular Diffusion Coefficient	0.5	- 2.5	$\mu m^2/ms$	[49, 54–56]	*†
Intracellular T_2 Relaxation Time	20	- 40	ms	[8, 54–56, 68–70]	*
Extracellular T_2 Relaxation Time	80	- 140	ms	[54, 55, 68, 69]	*
B-Value	300	- 1200	s/mm^2	[8, 25, 44, 71]	*†
Diffusion Time	10	- 90	ms	[25, 71]	*
	10	- 750	ms	[19, 20, 72]	†

List of Figures

Figure 1 (a) Effective dMRI sequence and (b) periodic muscle fiber model. Solid rectangle designates the cross-section of the representative elementary volume (REV) in the x-y plane. 20

Figure 2 (a) First-order indices and (b) total-order indices for dMRI signal simulations with no added noise (color bars) and with added SNR levels of 10 (▽), 25 (⋆), 50 (o) and NSA = 1. Error bars are confidence intervals. 21

Figure 3 Sum of L2-norm difference between the first-order sensitivity indices for the noise-free results and when synthetic noise is added for different NSA (left panels) and SNR levels (right panels). Colors denote the SNR level for a single acquisition. The dotted lines in the right panels are power law regressions ($\sim SNR^{\alpha}$) and R^2 is the correlation coefficient. 22

Figure 4 First and total-order indices for dMRI signal simulations of the generalized diffusion–weighted pulse sequence. Error bars are confidence intervals. 23

List of Tables

Table 1 Range of input parameters used in sensitivity study for both PGSE and the generalized diffusion sequence; parameters span range of experimentally observed values. * denotes parameters used in the sensitivity analysis of the PGSE sequence while † denotes parameters used in the analysis of the generalized diffusion-weighted sequence. T_2 ranges include reported values for field strengths between 0.5 - 7T. 24

Supporting Information

Supporting Information Figure S1: Relative error of LBM model integrated over a homogeneous domain for different relaxation factors.

Supporting Information Table S1: A list of all first, second and total-order sensitivity indices for the PGSE sequence.

Supporting Information Table S2: A list of all first, second and total-order sensitivity indices for the generalized-weighted diffusion-weighted sequence.

Supporting Information Table S3: Results of simple sensitivity analysis of two compartment diffusion model for changes in parameter ranges. Four different cases are examined: a) standard parameter range, b) change in volume fraction, c) change in T_2 values and d) change in diffusion coefficients.